Available online at www.sciencedirect.com
ScienceDirect
Coordination Chemistry Reviews 251 (2007) 925–935
COORDINATION CHEMISTRY REVIEWS
www.elsevier.com/locate/ccr

Review

Non-hydride systems of the main group elements as hydrogen storage materials

Henrietta W. Langmi, G. Sean McGrady *

Department of Chemistry, University of New Brunswick, Fredericton, NB E3B 6E2, Canada

Received 2 May 2006; accepted 17 September 2006
Available online 27 September 2006

Contents

Abstract

This review surveys the state of the art in non-hydride hydrogen storage materials composed of the elements B, C, N, O, Si, and Al. In the nitrogen-based systems Li_3N and NH_3BH_3 hydrogen is chemically bound in the formal oxidation states +1 and −1, whereas carbon nanotubes and aluminosilicate-based zeolites adsorb or encapsulate molecular H_2. The advantages and drawbacks of each system are discussed, and comparisons between them are made where appropriate.

Keywords: Hydrogen storage materials; Lithium nitride; Ammonia borane; Zeolites; Carbon nanotubes

1. Introduction

There are no problems more immediate and important to our 21st century lifestyle than the dwindling reserves of hydrocarbon fuel resources and the concomitant environmental impact of burning fossil fuels. Since the concept of a 'hydrogen economy' was proposed following the oil shocks of the 1970s there has been on-going research across the globe aimed towards a viable hydrogen economy. However, this effort has acquired increased immediacy and urgency over the past decade.

One of the main obstacles to a viable hydrogen fuel economy is the storage and transportation of the material. Compression of H_2 is energy-intensive and carries associated safety risks, and the liquefaction of the gas carries a concomitant energy penalty (H_2 boils at 20 K), quite apart from the low volumetric energy density – only one-quarter that of gasoline – associated with the low density of the liquid. Accordingly, it is widely recognised that a chemical solution is required for the satisfactory storage of hydrogen.

In 2004, the US Department of Energy (DOE) published a landscape document [1] that set out the following desiderata for a hydrogen storage technology appropriate for transportation:

1. High hydrogen storage capacity (min 6.0 wt.% H).
2. Low H_2 generation temperature (T_{dec} ideally around 60–120 °C).
3. Favourable kinetics for H_2 adsorption/desorption.
4. Low cost.
5. Low toxicity and low hazards.

The first of these requirements effectively limits chemical solutions to about a dozen light elements, as detailed in Fig. 1

* Corresponding author.
E-mail address: smcgrady@unb.ca (G.S. McGrady).

0010-8545/$ – see front matter © 2006 Elsevier B.V. All rights reserved.
doi:10.1016/j.ccr.2006.09.009

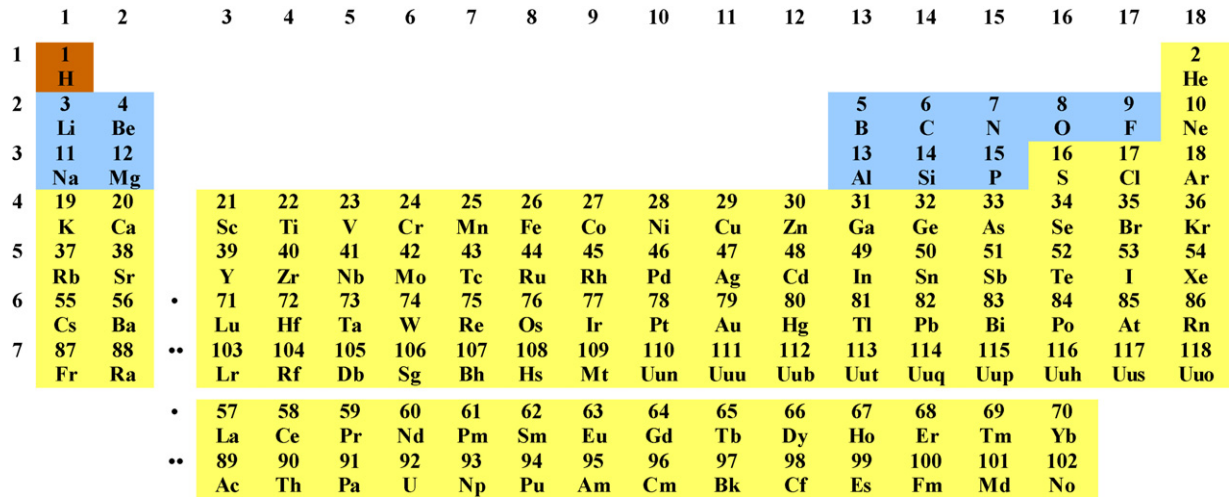

Fig. 1. Position of hydrogen in the periodic table, and set of elements (in blue) that should constitute a lightweight backbone of a hydrogen storage material to meet fundamental economic criteria. Redrawn with permission from [2]. Copyright 2004 American Chemical Society. (For interpretation of the references to colour in this figure legend, the reader is referred to the web version of the article.)

[2]: although many transition metals form polyhydrides and molecular hydrogen complexes with a high chemical content of hydrogen, the mass of the metal vitiates most of these advantages. For example, the stable polyhydride complex $BaReH_9$ is 81%H by elemental composition, but only 2.7%H by weight. Major research programs are focused on the hydrides and complex hydrides of the light metals shown in Fig. 1. For example, the systems MgH_2, AlH_3 and $NaAlH_4$ contain 7.6, 10.0 and 7.4 wt.% H, respectively, satisfying criterion 1. However, in spite of these advantages [3,4] each of these systems has drawbacks in terms of reversibility, or the temperature at which H_2 is released or reabsorbed. There have been excellent recent reviews documenting the efforts being made to develop transition metal and main group hydrides as hydrogen storage materials [2,5].

In addition to these light metal hydride systems, there exist several compounds and materials of the main group elements with attractive properties and the potential to do the same job, albeit in a different way. For example, lithium nitride, Li_3N, reacts with hydrogen gas to form a mixture of LiH and $LiNH_2$, which subsequently releases H_2 upon heating. Here the hydrogen molecule has been cleaved heterolytically, with one half ending up as lithium hydride and the other half as part of an amide anion. Ammonia borane, NH_3BH_3, stores H_2 in a similar way: the acidic N–H and basic B–H moieties in this molecule set up strong proton–hydride hydrogen-bonding interactions in the solid which facilitate the formation and release of H_2. Carbon nanotubes have a high surface energy and a strong affinity for binding small molecules: the physi- and chemisorption of molecular hydrogen by these nanoscale carbon species is significantly greater than by graphite. Finally, zeolites based on an aluminosilicate cage structure contain pores and channels with dimensions similar to those found in carbon nanotubes, and can bind and sequester molecular H_2 in a similar manner.

This review collates the current state of knowledge of these four chemically diverse types of main group system, and discusses their merits and drawbacks as potential hydrogen storage materials in the light of current US DOE requirements.

2. Lithium nitride, Li_3N

The reaction of Li_3N with H_2 was reported in the early part of the 20th century [6]. However, interest in Li_3N as a hydrogen storage material only began recently when Chen et al. [7] investigated its reversible hydrogen uptake. The hydrogenation process occurs in two steps [8]:

$$Li_3N + H_2 \leftrightarrow Li_2NH + LiH, \quad \Delta H = -116\,kJ/mol \quad (1)$$

$$Li_2NH + H_2 \leftrightarrow LiNH_2 + LiH, \quad \Delta H = -45\,kJ/mol \quad (2)$$

The structure of α-Li_3N, shown in Fig. 2(a) [9], consists of graphite-like layers of Li hexagons with a nitride ion at the centre of each. These Li_6N hexagons are capped by two further Li ions above and below the plane, resulting in an Li_8N hexagonal bipyramidal arrangement [10,11]. The initial stages of reaction between lithium nitride and deuterium gas have been explored by neutron diffraction [12]: at a composition of $Li_{2.95}ND_{0.02}$, the deuterium atoms bind initially to the nitride, giving disordered ND^{2-} ions within the parent Li_3N structure; Fig. 2(b). X-ray diffraction analysis of hydrogenated Li_3N shows distinct LiH and $LiNH_2$ phases [7].

Lithium nitride has a high theoretical hydrogen uptake capacity of 11.5 wt.%, which makes it attractive as a hydrogen storage material. The investigation by Chen et al. [7] showed that the absorption of H_2 by a fresh Li_3N sample begins at approximately 100 °C (Fig. 3). A total hydrogen storage capacity of 9.3 wt.% is attained after maintaining the sample at 255 °C for 30 min. Under high vacuum and at temperatures below 200 °C, about 6.3 wt.% H_2 is desorbed. Complete desorption is achieved when the temperature is raised above 320 °C. In another study, Hu and Ruckeinstein [13] reported that Li_3N has an initial hydrogenation temperature of about 150 °C, which is independent of the hydrogen concentration in the reactant gas stream. The temperature-programmed-dehydrogenation curve of the sample hydrogenated at 300 °C shows three hydrogen peaks at 240, 270 and above 380 °C. The two low temperature peaks correspond to

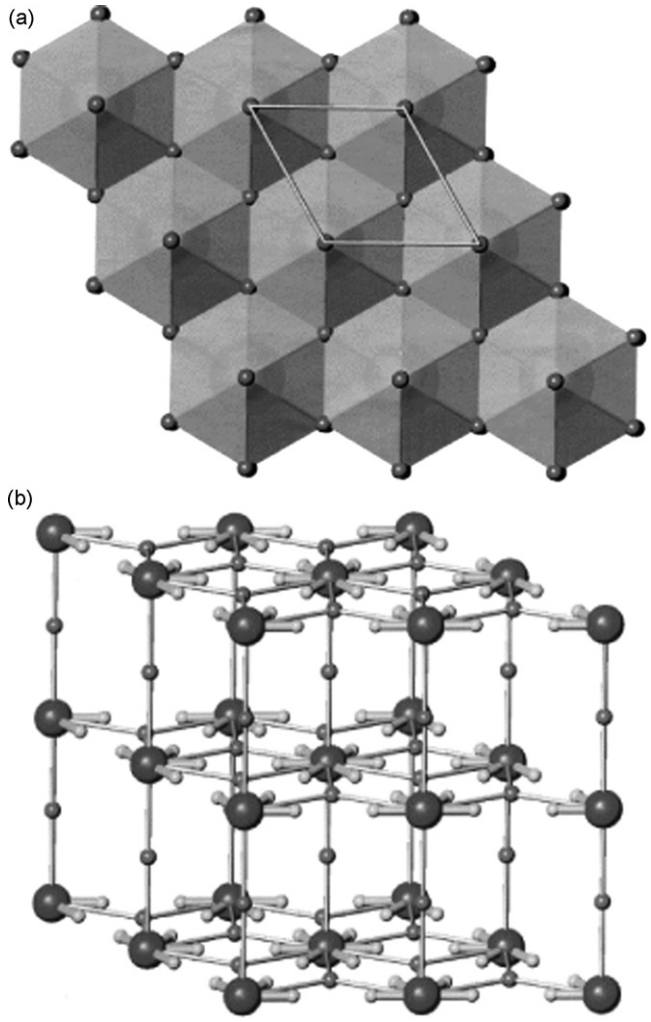

Fig. 2. Polyhedral representation of the structure of α-Li_3N (a) as a projection on the [0 0 1] plane showing [Li_2N] layers of edge-sharing NLi_8 hexagonal bipyramids; (b) structure of $Li_{3-x-y}ND_y$ ($y \approx 0.02$). The deuterium-doped nitride retains the space group of Li_3N (*P6/mmm*) with D (smallest light spheres) disordered in the 6*j* position (0.19(4)% occupied). Lithium atoms are depicted as small spheres, N as large spheres. Reprinted with permission from [9]. Copyright 2001 Elsevier.

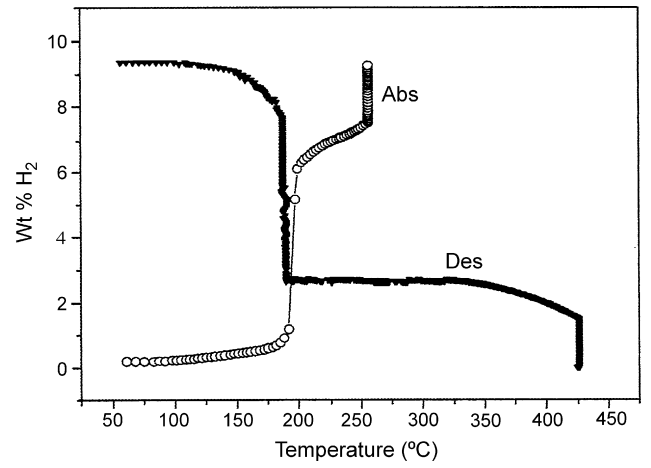

Fig. 3. Weight variations during hydrogen absorption and desorption processes over Li_3N samples. Abs, absorption; Des, desorption. Reprinted with permission from [7]. Copyright 2002 Nature Publishing Group.

the transformation of $LiNH_2$ to Li_2NH. Meanwhile, the transformation of Li_2NH back to Li_3N is responsible for the third peak.

Some of the important characteristics of a hydrogen storage system are fast kinetics, good reversibility and stability. When Li_3N is reacted with H_2 it achieves a rapid weight gain between 170 and 210 °C [7]. At about 160 °C the reaction is sluggish and incomplete, reaching a storage capacity of ≈7.0 wt.% [14]. Due to the partial dehydrogenation of hydrogenated Li_3N, its reversible hydrogen storage capacity is about 5.5 wt.% at 280 °C or lower [15]. The full reversal of the hydrogenation reaction of Li_3N is not an easy process and often requires high temperatures and long periods [7,13,16]. The recovered Li_3N from dehydrogenation at 400 °C has a very low rehydrogenation capacity of 0.4 wt.%. Such high temperatures result in sintering of the regenerated Li_3N, diminishing its effectiveness as a hydrogen storage medium [15]. Deactivation of Li_3N as a result of sintering can also occur during hydrogenation [8,17]: this is an exothermic process and the fast absorption during the first several minutes of the initial hydrogenation causes a large temperature jump that leads to sintering [8]. Various approaches have been taken to prevent the deactivation of Li_3N in order to improve its stability [17,18]. By partially oxidizing Li_3N and subsequently performing a hydrogenation-dehydrogenation pretreatment, Hu and Ruckenstein [17] reported that reversible 5.0 wt.% H_2 can be achieved in only 3 min at 180 °C by the resulting Li_2O/Li_3N material. In addition, the reversible hydrogen storage capacity and absorption rate does not decrease after six cycles at 198 °C, indicating that the Li_2O/Li_3N system possesses both fast kinetics and excellent stability. Preheating Li_3N in vacuum at 400 °C is also effective in improving its hydrogen storage stability [8]. Furthermore, enhancement of the reversible hydrogen storage capacity of Li_3N can occur when $LiNH_2$ is added to Li_3N [18].

One aspect of critical importance associated with the Li–N–H system is the possibility of generating ammonia during hydrogenation and dehydrogenation of the material [16,19]. In fact, NH_3 formation is thermodynamically favourable at temperatures below 400 °C [16]. Hino et al. [20] concluded that about 0.1% NH_3 inevitably contaminates the hydrogen desorbed from a mixture of LiH and $LiNH_2$ at any temperature up to 400 °C in a closed system. Ammonia also plays a mediating role in the hydrogen desorption reaction (Eq. (2)), which consists of two elementary steps [16,21]:

$$2LiNH_2 \rightarrow Li_2NH + NH_3, \qquad \Delta H = +84\,kJ/mol \qquad (3)$$

$$LiH + NH_3 \rightarrow LiNH_2 + H_2, \qquad \Delta H = -42\,kJ/mol \qquad (4)$$

Hu and Ruckenstein [16] claimed reaction (4) is ultra-fast; NH_3 released from reaction (3) is totally captured by LiH in reaction (4) even when contact is only for 25 ms. As a result of the speed at which reaction (4) occurs, NH_3 formation during the hydrogenation of Li_3N is suppressed and NH_3 generated during the dehydrogenation process is prevented from contaminating the H_2 gas emitted. Pinkerton illustrated that in a dynamic H_2 atmosphere, a slow but significant decomposition of $LiNH_2$ by NH_3 release occurs [22]. Under a static gas atmosphere the

formation of NH_3 is self-limiting. While some studies have detected no NH_3 during the hydrogenation/dehydrogenation of Li_3N [13], others have reported small amounts of NH_3 emission [14].

Some researchers have focused their investigations on the reversible reaction between $LiNH_2$ and LiH (Eq. (2)), because this reaction has a smaller enthalpy change and can therefore absorb/desorb 6.5 wt.% H_2 more readily [20,21,23,24]. Chen et al. [19] reported that when $LiNH_2$ and LiH are thoroughly mixed, H_2 is released at temperatures around 150 °C. Depending on the temperature and molar ratio of $LiNH_2$/LiH, the solid products can be Li_2NH, Li_3N and Li-rich imide. Ichikawa et al. [21,23] examined the effect of catalysts on the desorption properties of ball-milled mixtures of $LiNH_2$/LiH (1:1 molar ratio) with 1 mol% of various catalysts such as Fe, Co, or Ni nanoparticles, $TiCl_3$ and $VC1_3$. The desorption spectra of the ball-milled sample without catalyst addition showed that H_2 is released between 180 and 400 °C with a significant amount of NH_3 emission [23]. The mixture containing 1 mol% $TiCl_3$ exhibits the best H_2 desorption properties, releasing approximately 5.5–6.0 wt.% H_2 at 150–250 °C with relatively fast kinetics and good reversibility, and no release of NH_3 [21]. The particle size of added catalysts has been reported to influence the catalytic effect on the hydrogen storage properties of $LiNH_2$/LiH [24]. The hydrogen storage properties of Li_3N may also be affected if the hydrogenated material (i.e. $LiNH_2$ and LiH) is exposed to air [16,21].

One way of enhancing the dehydrogenation reaction of $LiNH_2$ (Eq. (2)) is to partially substitute Li with other elements of higher electronegativity, such as Mg (Pauling electronegativities: Li = 0.98; Mg = 1.31) [25–27]. Charge compensation by the Li^+ cation is a major factor in the destabilization of the $[NH_2]^-$ anion, and substitution with a more electronegative element weakens the ionic interaction with this anion [26]. For $LiNH_2$ that has been partially substituted with 10 mol% Mg, the H_2 desorption temperature is significantly lower relative to that of unsubstituted $LiNH_2$ [28], and this temperature decreases with increasing Mg content [26]. Several investigations of the Li–Mg–N–H storage system (i.e. a combination of $Mg(NH_2)_2$ and LiH) have been carried out [29–33]. Ichikawa et al. [29] examined the isothermal hydrogen absorption properties of a 3:8 molar mixture of $Mg(NH_2)_2$ and LiH. The mixture was first ball-milled and dehydrogenated at 200 °C under high vacuum. The P–C–T curve at 200 °C showed a two-plateaux-like behaviour and attained the fully hydrogenated state under 9 MPa H_2. Meanwhile, the P–C–T curve at 150 °C exhibited single-plateau-like behaviour and only reached a partially hydrogenated state under the same H_2 pressure. Another study on a 3:8 molar mixture of $Mg(NH_2)_2$ and LiH showed that the mixture starts to desorb hydrogen at 140 °C, recording a peak desorption at 190 °C, with almost no NH_3 emission [30]. The system was reported to have superior qualities in terms of hydrogen storage to one of $LiNH_2$ and LiH [30]; it can reversibly absorb/desorb about 7.0 wt.% H_2 at moderate temperature and pressure:

$$3Mg(NH_2)_2 + 8LiH \leftrightarrow Mg_3N_2 + 4Li_2NH + 8H_2 \quad (5)$$

It was later reported that reaction (5) actually consists of a series of intermediate reactions mediated by NH_3 [31]. A mixture of $Mg(NH_2)_2$ and LiH in a molar ratio of 1:4 has also been studied [32].

A wide range of other amide–hydride systems has been studied, including $Mg(NH_2)_2$ and MgH_2 [32]; $LiNH_2$ and MgH_2 [33]; $Mg(NH_2)_2$ and NaH [34]; $Ca(NH_2)_2$ and CaH_2 [35]; $LiNH_2$ and $LiBH_4$ [36,37]; and $LiNH_2$ and $LiAlH_4$ [38]. It is noteworthy that $LiNH_2$ has been demonstrated to destabilize $LiBH_4$ [36] and $LiAlH_4$ [38]; the latter two compounds are regarded as promising hydrogen storage materials because of their very high hydrogen content. In general, the temperature at which H_2 desorption occurs in amide–hydride systems is significantly lower when compared to the decomposition temperature for the corresponding pure amide and hydride. For instance, the decomposition temperatures for $LiNH_2$ and LiH are 300 and 550 °C, respectively, but a mixture of these two compounds releases H_2 at about 150 °C [19]. A better understanding of the chemical interactions between amides and hydrides will almost certainly be of value in the search for a new metal–N–H storage system.

3. Ammonia borane, NH_3BH_3

B–N–H compounds of general formula NH_xBH_x have high theoretical hydrogen capacities of 24.5, 19.6, 14.0 and 7.5 wt.% for $x = 4$, 3, 2 and 1, respectively [39]. These compounds are inorganic analogues of hydrocarbons. In fact, based on the main groups of aliphatic hydrocarbons the B–N–H system can be subdivided into three classes; namely, amineboranes (empirical formula NH_3BH_3), aminoboranes (NH_2BH_2) and borazines (NHBH) [40]. While the hydrocarbons are gases at room temperature, their inorganic analogues are solids on account of the difference in electronegativity between the B and N atoms and the stronger interactions between the molecules in the B–N–H compounds [39]. The crystal structure of ammonia borane has been determined by neutron diffraction [41], and is shown in Fig. 4. The precursor to ammonia borane – ammonium borohydride, NH_4BH_4 – is a white crystalline solid that decomposes at temperatures above −40 °C to give H_2 and a solid of composition $[BNH_6]_x$ believed to be the "diammoniate of diborane" [42]. Decomposition of NH_4BH_4 is half-complete after 6 h at room temperature [42], making this compound unattractive as a hydrogen reservoir on account of its instability. Grochala and Edwards [2] reasoned that the ease with which the decomposition of NH_4BH_4 occurs cannot arise solely from the thermodynamic instability of the isolated NH_4^+ and BH_4^- subunits, but that the attractive interaction between the N–H and B–H moieties lowers the activation energy for hydrogen evolution and facilitates the decomposition (cf. the structure of NH_3BH_3; Fig. 4).

Ammonia borane (or borazane), NH_3BH_3 is also a white, crystalline, ether-soluble solid, which slowly "splits out hydrogen" at room temperature [43,44]. The fact that NH_3BH_3 is a crystalline solid at room temperature, whereas the isoelectronic CH_3CH_3 boils at −80 °C, can be attributed in large part to the strong proton–hydride hydrogen bonding [45] between the posi-

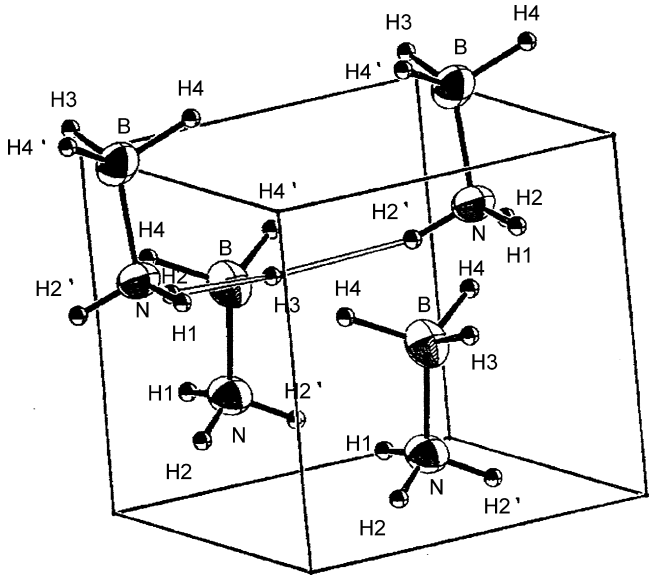

Fig. 4. Neutron diffraction structure of NH_3BH_3, with the shortest intermolecular H···H contacts [H_2–H_3, 2.02(3) Å] indicated. Reprinted with permission from [41]. Copyright 1999 American Chemical Society.

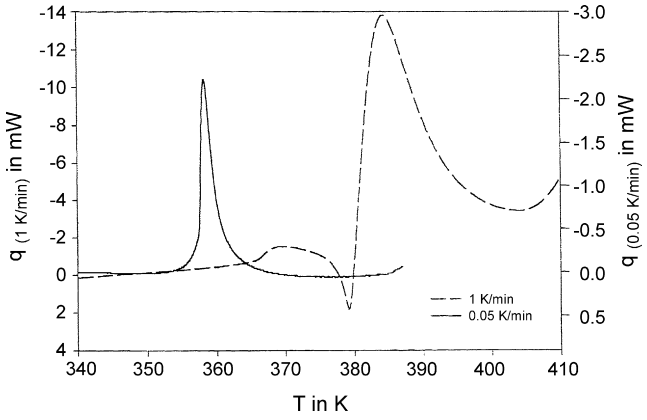

Fig. 5. DSC plots of the thermal decomposition of NH_3BH_3: (—) heating rate 0.05 K/min and (···) heating rate 1 K/min. Reprinted with permission from [47]. Copyright 2000 Elsevier.

tively charged N–H and negatively charged B–H moieties, which is evident in the short H···H contacts revealed in Fig. 4.

In the 1950s, several synthetic routes to NH_3BH_3 were reported [43,44]. One approach involves reacting $LiBH_4$ with NH_4CI or $(NH_4)_2SO_4$ in diethyl ether. Another route involves the reaction between "diammoniate of diborane" and NH_4CI in diethyl ether with a trace of NH_3. Other approaches, including the reaction of $NaBH_4$ with either $(NH_4)_2CO_3$ or CO_2 and NH_3 in THF, have also been reported [46]. Ammonia borane is a potential candidate for hydrogen storage owing to its high hydrogen content, its moderate temperature for H_2 release and the exothermic nature of the decomposition reactions [47–49]. However, the thermal decomposition of NH_3BH_3 is a complex process that involves a series of sequential reactions [50]:

$$NH_3BH_3 \rightarrow NH_2BH_2 + H_2, \qquad 6.5\,wt.\% \tag{6}$$

$$xNH_2BH_2 \rightarrow (NH_2BH_2)_x \tag{7}$$

$$(NH_2BH_2)_x \rightarrow (NHBH)_x + H_2, \qquad 6.9\,wt.\% \tag{8}$$

Differential thermal analysis (DTA) studies of NH_3BH_3 reveal features at about 125 and 155 °C, attributed to the spontaneous formation of polymeric aminoborane $(NH_2BH_2)_x$ (Eqs. (6) and (7)), and its subsequent decomposition (Eq. (8)), respectively [50]. Temperatures in excess of 500 °C are needed to release the final equivalent of H_2 from polymeric iminoborane $(NHBH)_x$ to form boron nitride [44].

Above its melting point of 112–114 °C, ammonia borane decomposes vigorously with the release of H_2, [51]. The decomposition process proceeds in stages as the temperature is increased to 200 °C, generating a white residue [51]. Two partially overlapping exothermic steps are involved in the evolution of H_2 during the thermal decomposition of NH_3BH_3 [47,48]. At high heating rates the first exothermic process corresponding to the first decomposition step begins at approximately 95 °C (368 K). Immediately after the start of this exothermic event, an endothermic event attributed to the melting of NH_3BH_3 partially compensates the exothermic process (Fig. 5). Then, just before the first exothermic process is complete, another exothermic process corresponding to the second decomposition step begins. Both exothermic steps can be clearly separated under isothermal conditions or at low heating rates (Fig. 5) [47,48]. Wolf et al. [47] reported that NH_3BH_3 can totally decompose below its melting point under suitable conditions. Low heating rates or isothermal conditions are necessary for the separation of the two exothermic steps because of the low decomposition rate of NH_3BH_3. In this way, the first decomposition step completely ends before the second step begins. The first decomposition step releases 1.0 mol H_2/mol NH_3BH_3, corresponding to 6.5 wt.% H_2 [47]. This value is obtained after approximately 6 h at 90 °C and after more than 40 h at 70 °C. The enthalpy change for the decomposition reaction is about −21.7 kJ/mol NH_3BH_3. At about 180 °C a total of ≈2.2 mol H_2/mol NH_3BH_3 is released, corresponding to 14.3 wt.% H_2 [48]. This value does not change at higher temperatures. However, the amount of gaseous products evolved along with H_2 increases with higher heating rates [48,49]. Other products resulting from the thermal decomposition of NH_3BH_3 are $(NH_2BH_2)_x$ solid residue, and gaseous compounds including monomeric aminoborane (NH_2BH_2), borazine ($B_3N_3H_6$) and traces of diborane (B_2H_6). Borazine is mainly released only above 130 °C [48].

Monomeric aminoborane polymerizes spontaneously between −196 and −155 °C [52]. It is possibly a reactive intermediate involved in the formation of $B_3N_3H_6$ by pyrolysis of NH_3BH_3 [48]. Iminoborane, NHBH is a highly reactive precursor to $B_3N_3H_6$ [48,53]. Borazine is isoelectronic with benzene, and the two molecules bear close similarities with each other, as evidenced by their physical and spectral properties [54]. Polymeric aminoboranes are inorganic analogues of polyethylene that could be cyclic or chain-like [40,55]. The cyclic forms are thermally much more stable than the linear species [40].

The main disadvantage of NH_3BH_3 as a hydrogen storage material is its irreversibility: upon releasing H_2 it converts into

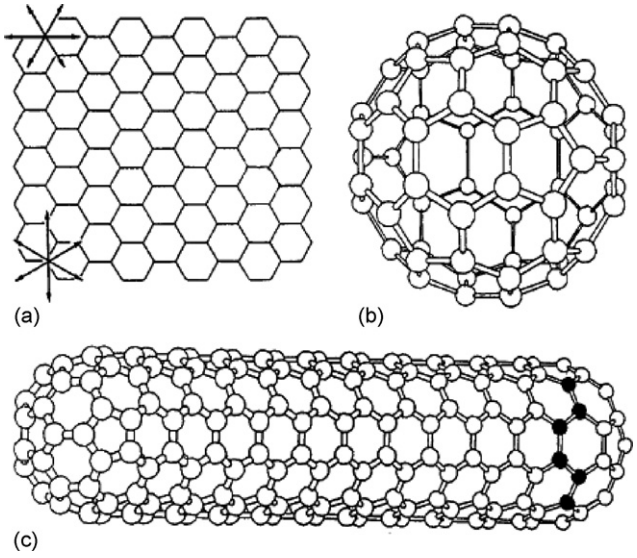

Fig. 6. Stable forms of carbon clusters: (a) a piece of graphene sheet, (b) the fullerene C_{60} and (c) a model for a carbon nanotube. Reprinted with permission from [57]. Copyright 1997 Annual Reviews.

a series of intermediates, which are unsuitable for the release of subsequent equivalents of H_2. Recently, Gutowska et al. [39] have shown that a nanophase scaffold of mesoporous silica, SBA-15, loaded with NH_3BH_3 significantly enhances the hydrogen storage properties of this material. Hydrogen is released from NH_3BH_3 in the scaffold at a much lower temperature than for pure NH_3BH_3: release of the first equivalent of H_2 from the pure material occurs at 110 °C, whereas NH_3BH_3 in the scaffold evolves H_2 below 100 °C. In addition, less borazine is produced from the scaffolded material. The enthalpy of reaction for H_2 loss is considerably less exothermic (≈−1 kJ/mol) for NH_3BH_3 in the scaffold than for pristine NH_3BH_3 (≈−21 kJ/mol), implying that the reverse reaction is more favourable for the former material. There is a difference in the non-volatile products formed in each case. The study also showed that the scaffolded NH_3BH_3 has a much lower activation barrier. More recently, the effects of milling and doping on the decomposition of NH_3BH_3 have been studied [56]. Benedetto et al. [56] claimed that NH_3BH_3 doped with 1 mol% Pt has a lower decomposition temperature than pristine NH_3BH_3, making it more suitable for the working temperature of a PEM fuel cell. In the light of these latter two studies [39,56], it seems likely that there is room for further advances in the development of NH_3BH_3 as a hydrogen storage material.

4. Carbon nanotubes/nanofibres

Carbon nanotubes (CNTs) consist of graphene sheets rolled up into a cylindrical shape with a diameter on the nanometer scale and a length of tens of microns. When produced, CNTs are usually closed at each end by hemispherical fullerenes. Fig. 6 shows a schematic representation of a graphene sheet, a fullerene and a CNT [57]. There are basically two types of CNTs: single-walled nanotubes (SWNTs) and multi-walled nanotubes (MWNTs). SWNTs are formed from a single graphite layer and have the tendency to self-organize into ropes via van der Waals interactions during synthesis [58]. Nanotubes formed from multiple nested concentric layers of graphite are referred to as MWNTs. Nanotubes (MWNTs) were first discovered accidentally during fullerene synthesis when carbon was vaporized in an electric arc [59]. SWNTs were later discovered in 1993 [60] and since then numerous reports have been published – with conflicting results – on the potential of CNTs as hydrogen storage materials. What distinguishes CNTs from high surface area graphite is the curvature of the graphene sheets and the hollow space within the nanotube. In microporous solids with pores no larger than a few molecular diameters, the potential fields from the walls of the micropores overlap to give stronger gas–solid interactions than would occur for adsorption on a flat carbon surface; this is the impetus behind current investigation of CNTs for hydrogen storage [61]. Recent reviews of hydrogen storage in CNTs have been published [62,63].

Hydrogen storage in CNTs can occur by physisorption or chemisorption. Several theoretical studies have been reported detailing physisorption and chemisorption calculations on hydrogen in CNT [64–72]. Lee and Lee [67] performed density functional-based calculations to search for adsorption sites and predict maximum hydrogen storage capacity. This study identified two chemisorption sites; top sites at the exterior and interior of the nanotube wall. It was also found that hydrogen molecules can be located in the empty space inside the nanotube (Fig. 7). The results further demonstrated that hydrogen storage capacity increases linearly with tube diameter in SWNTs. Simonyan and Johnson [72] investigated the influence of nanotube spacing on hydrogen uptake, and suggested that at low pressures kinetic effects or impurities in the sample might limit access by hydrogen to some nanotubes. However, at high pressures hydrogen may cause the nanotube ropes to swell, blocking the entrances to the nanotubes. The amount of hydrogen adsorbed on CNTs has been reported to be a function of surface area and temperature [73,74]. Unsurprisingly, hydrogen adsorption at −196 °C was found to be significantly greater than at room temperature. At cryogenic temperatures, physisorption appears to be the mechanism of hydrogen adsorption. However, at elevated temperatures, hydrogen can become covalently bonded to carbon, and hydrocarbons were detected in the desorption spectrum.

In 1997 the first experimental results on hydrogen adsorption in CNTs were published by Dillon et al. [75]. In this study, arc-generated soot containing 0.1–0.2 mass% SWNTs was investigated at ambient temperature and pressure conditions. The measured hydrogen desorption was only 0.01 wt.% for the whole sample. It was assumed that only the SWNTs in the sample contributed to hydrogen adsorption. The authors therefore extrapolated a hydrogen storage capacity of 5–10 wt.% for a pure SWNT sample. As a follow-up to the work of Dillon et al. [75], Ye et al. [76] carried out hydrogen measurements on a much purer sample of SWNTs. Hydrogen adsorption on the ropes of SWNTs was found to exceed 8 wt.% at 120 bar and about −196 °C. It was concluded that hydrogen was first adsorbed on the outer surfaces of the crystalline ropes, then at pressures above ∼40 bar a phase transition occurred where the individual SWNTs became separated and hydrogen was able to penetrate

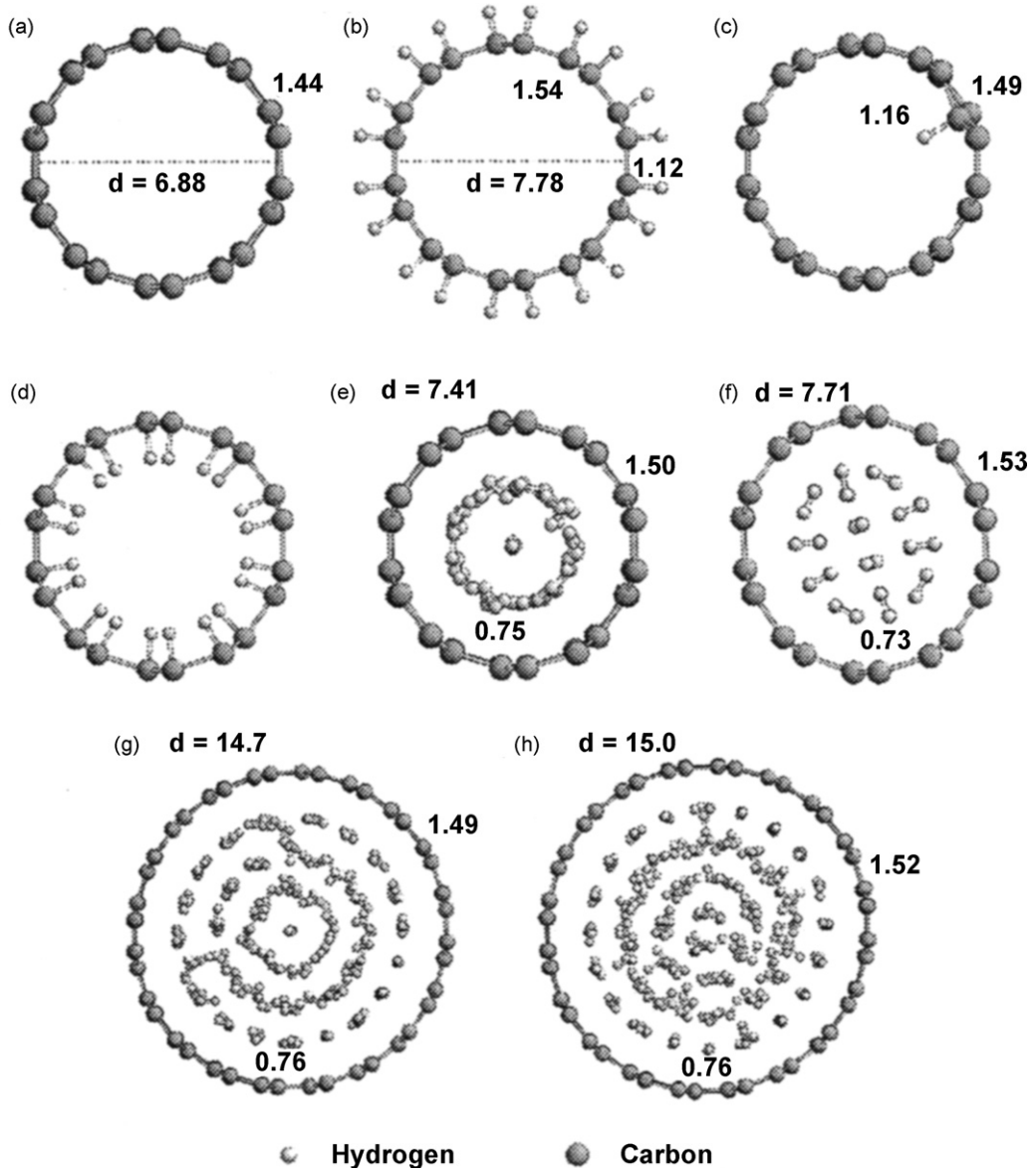

Fig. 7. Top views of various hydrogen adsorptions in SWNTs: (a) clean (5,5) CNT; (b) hydrogen atoms adsorbed at the exterior of the tube wall with $\theta = 1.0$; (c) adsorption of a single hydrogen atom at the interior of the wall; (d) the initial geometry of hydrogen atoms adsorbed at the interior of the wall with $\theta = 1.0$; (e) the fully relaxed geometry of (d); (f) H_2 inside the tube with $\theta = 1.2$; (g) H_2 inside (10,10) the CNT with $\theta = 2.0$; (h) with $\theta = 2.4$. Bond lengths are in Å. Reprinted with permission from [67]. Copyright 2000 American Institute of Physics.

the newly exposed surfaces of the nanotubes. Nevertheless, this phenomenon could not account for the high wt.% values at ambient conditions. Further work by Dillon et al. [77] reported 7 wt.% reversible hydrogen storage in high purity SWNTs opened by an ultrasonic cutting procedure that incorporates a $TiAl_{0.1}V_{0.04}$ alloy. Hirscher et al. [78] later revealed that such a treatment procedure leads to an incorporation of Ti particles in the sample. Most of the hydrogen storage was attributed to the Ti metal particles. At room temperature and 100 bar, a hydrogen uptake value of 4.2 wt.% was reported for SWNTs with large mean diameters of 1.85 nm [79].

Graphite nanofibres (GNFs) bear close similarities with CNTs, but differ in the arrangement of the graphite platelets around the fibre axis [80]. An extraordinarily high hydrogen storage capacity, exceeding 67 wt.% at ~112 bar and room temperature, has been reported for GNFs [80]. It was claimed that the large hydrogen uptake arose from the special geometry of the samples, providing a large proportion of edge sites for hydrogen adsorption. However, these results remain highly controversial: to date, they have not been reproduced. For instance, Ahn et al. [81] investigated various GNFs and the desorbed hydrogen was generally below 0.08 wt.%. In yet another attempt to corroborate the ambitious claims of Chambers et al. [80] a maximum hydrogen storage capacity of only 1.5 wt.% was achieved for GNFs at 125 bar and room temperature [82].

Chen et al. [83] have reported considerable hydrogen uptake in alkali metal-doped MWNTs prepared by catalytic decomposition of CH_4. The study concluded that a high hydrogen uptake of 14 and 20 wt.% could be achieved for K- and Li-doped MWNTs respectively at a pressure of 1 bar. While the K-doped

MWNTs were chemically unstable and adsorbed hydrogen at room temperature the Li-doped MWNTs were chemically stable and required temperatures between 200 and 400 °C. It was suggested that hydrogen adsorption occurred by dissociation catalyzed by the intercalated alkali metal in the MWNTs. In another investigation, Yang [84] carried out a TGA study on MWNTs prepared using the same procedure as employed by Chen et al. [83]. K-doped MWNTs showed a weight increase of only 1.8 wt.% when exposed to 'dry' hydrogen. Meanwhile, Li-doped MWNTs showed a weight increase of 12 wt.% when exposed to 'wet' hydrogen and 2.5 wt.% in 'dry' hydrogen. The IR spectrum obtained by Chen et al. for this material was shown to resemble closely that of $LiOH{\cdot}H_2O$ [83]. The sensitivity of Li-doped samples to moisture has been subsequently confirmed [85].

A study by Wu et al. [86] was carried out on MWNTs synthesized by the catalytic decomposition of CO and CH_4 on powdered La_2C_3 catalysts. Thermogravimetric analysis showed that the CO-generated MWNTs were able to store 0.25 wt.% hydrogen when the sample was cooled between 200 °C and room temperature. More recently, Poirier et al. [87] reported hydrogen adsorption capacities for SWNTs; at 1 bar and −196 °C a value of 4 wt.% was reached. However, only 0.2 wt.% was attained at room temperature under the same pressure. Other recent studies have also reported hydrogen storage capacities of less than 1 wt.% at room temperature for CNTs [88,89]. Yamanaka et al. [90] investigated MWNTs and carbon nanofibres synthesized by CVD under a hydrogen gas atmosphere. They reported that hydrogen desorption began at 500 °C indicating that chemisorption was involved. Thermal desorption spectroscopy revealed hydrogen storage capacities of 8.6 and 0.77 wt.% for MWNTs and nanofibres respectively.

In spite of all the discrepancies in published data there is continued research interest in CNTs as hydrogen storage materials. It is now at least apparent that several factors, including synthesis route and purification procedure, hydrogen measurement technique, and sample purity and quality are likely responsible for the diversity in reported data.

5. Zeolites

Zeolites are highly crystalline aluminosilicate materials defined by a three-dimensional network of cavities and pores of molecular dimensions [91]. They are generally represented by the formula: $M_{x/n}[(AlO_2)_x(SiO_2)_y]{\cdot}mH_2O$, where M is a cation of valence n that neutralizes the negative charge on the aluminosilicate framework. The cations are bound electrostatically within the pores of the zeolite and are readily exchangeable. Some examples of framework structures are shown in Fig. 8 [92]. Zeolites have traditionally been used for decades in many industrial applications such as molecular sieving, catalysis, drying and ion exchange [93]. Zeolites are of interest as hydrogen storage media, and are advantageous over other microporous materials because they are cheap, readily available, easy to synthesize, highly robust, non-flammable in air or a hydrogen atmosphere and there exists a wide range of framework types. In addition, the ability of zeolites to undergo ion exchange provides a variety of chemical compositions and enables modification of the physical and chemical properties of these materials.

Hydrogen storage in zeolites can follow either an encapsulation mechanism or an adsorption regime. At elevated temperatures, encapsulation (sometimes referred to as trapping), is believed to occur [94,95]. At ambient temperatures, the pore entrances are not sufficiently activated to allow hydrogen molecules into the structure. However, at elevated temperatures and pressures hydrogen molecules are forced to penetrate the cavities as the apertures become activated. Subsequent cooling to room temperature and release of excess pressure causes the hydrogen molecules to become encapsulated (or trapped) within the pores: when the zeolite is reheated the hydrogen molecules are released [93,95]. One of the pioneering studies on hydrogen encapsulation in zeolites was carried out on zeolite A by Fraenkel and Shabtai [94]. Experiments were performed at 200–400 °C in the approximate pressure range 20–900 bar. Hydrogen encapsulation capacity increased with increase in ionic radius from Na^+ to K^+ but decreased for the larger Rb^+ and Cs^+ ions. The observed trend was explained by the decrease in effective critical pore size as the ionic radius increases, implying the encapsulate stability increased while the available intracrystalline void volume per gram of zeolite decreased. A similar trend was observed by Weitkamp et al. [95] for a loading temperature of 300 °C and pressure of 100 bar. CsA and RbA zeolites were found to be better hydrogen encapsulants as they retained most of their hydrogen on cooling to room temperature. An encapsulation capacity of 65 cm^3 (STP) g^{-1}, corresponding to

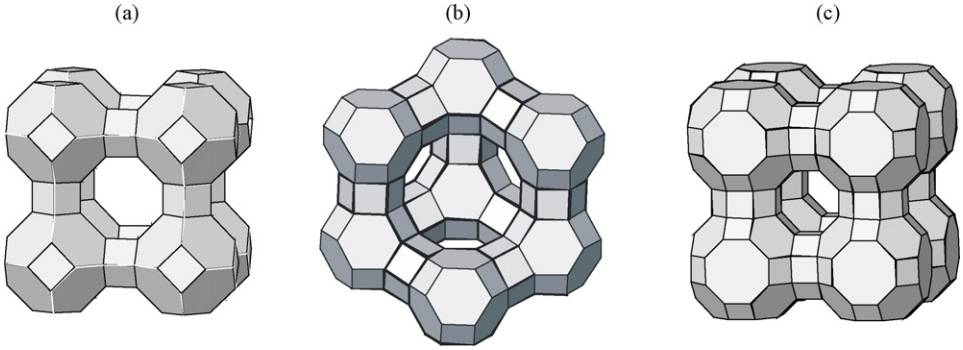

Fig. 8. Framework structures of zeolites: (a) zeolite A, (b) zeolites X and Y and (c) zeolite Rho. The corners on each framework represent Si or Al and these are linked by oxygen bridges represented by the lines on the frameworks. Reprinted with permission from [92]. Copyright 2003 Elsevier.

0.6 wt.% was reported for CsA when loaded at 300 °C and approximately 900 bar [94]. Further theoretical and experimental work on zeolite A carried out at 300 °C and 82 bar hydrogen pressure showed that zeolite A containing combinations of Cs^+ and Na^+ as exchangeable cations were most efficient in hydrogen trapping [96]. Fraenkel [97] later reported that encapsulation was restricted to the β-cages in NaA. Weitkamp et al. [95] reported a maximum storage capacity of 9.2 cm^3 (STP) g^{-1} (i.e. 0.08 wt.%) obtained for sodalite if loaded at 300 °C and 100 bar, and concluded that hydrogen encapsulation capacity was generally higher for zeolites having a reasonable portion of small cavities in their structure. Other hydrogen encapsulation studies on zeolite A [98,99] and Rho [100] have also been reported.

At room temperature, very high pressures are needed to attain significant hydrogen uptake in zeolites. For instance, Darkrim et al. [101] concluded that at room temperature and 700 bar, 100 hydrogen molecules per unit cell (corresponding to 1.2 wt.%) were stored in NaA. Nishimiya et al. [102] reported that when Pd nanoparticles or clusters are introduced in the pores of NaY they can hyperstoichiometrically occlude hydrogen. However, if the Pd content is too high Pd nanoparticles start to block the pores. At 1 bar and room temperature the hydrogen concentration was approximately 0.5 mmol g^{-1} (0.1 wt.%) for 7 wt.% Pd–NaY at room temperature. Kayiran and Darkrim [103] studied hydrogen adsorption on NaA, LiA and KA zeolites and their compacted forms. Hydrogen uptake at 10 bar and room temperature was approximately 0.1 wt.%. When the zeolites were compacted and measured at 60 bar and room temperature the hydrogen uptake was enhanced by a factor of 4.

Hydrogen adsorption at −196 °C on sodium forms of faujasites with different Si/Al ratios in the framework was studied by Kazansky et al. [104] using barometric measurements and DRIFT spectra. The number of hydrogen molecules adsorbed per Na^+ ion was largest for the most basic NaX with a low Si/Al ratio of 1.05 and lowest for the less basic NaY with a high Si/Al ratio of 2.4. In fact, a hydrogen adsorption value of about 3.6×10^{21} molecules g^{-1} (corresponding to 1.2 wt.%) was reported for NaX at less than 1 bar. DRIFT spectra studies on LiX, CaX and NaY have also been performed [105,106], and it was reported that hydrogen interacted with the cations as well as basic oxygen of the zeolite framework [105]. Recent investigations on chabazite zeolite frameworks have been carried out, both theoretically [107] and experimentally [107–109]. It was reported that in H-SSZ-13 zeolite the high surface area, internal wall topology and available protons worked in concert in allowing hydrogen to condense inside the nanopores under suitable conditions [108]. Below room temperature physical adsorption dominates the hydrogen storage mechanism in zeolites. Hydrogen adsorption has been shown to correlate with BET surface area (Fig. 9) [110,111] as well as with micropore volume [110]. Nijkamp et al. [110] studied zeolites L, ZSM5 and ferrierite, and reported that the highest capacity obtained at −196 °C and 1 bar was 80 mL H_2 (STP) g^{-1} (0.72 wt.%) for zeolite ZSM5. Langmi et al. [92,111] systematically investigated zeolites X, Y, A, and Rho containing a variety of exchangeable cations. They obtained a hydrogen storage capacity of 2.19 wt.% for CaX at −196 °C and 15 bar. It was also shown that pore blocking by large cations occurred in zeolites A and Rho, restricting access of hydrogen molecules into the zeolite cages. On the other hand, due to the open nature of the framework of zeolites X and Y, access to the internal pore space was not obstructed by large cations. It was suggested that cations might act as binding sites for hydrogen molecules.

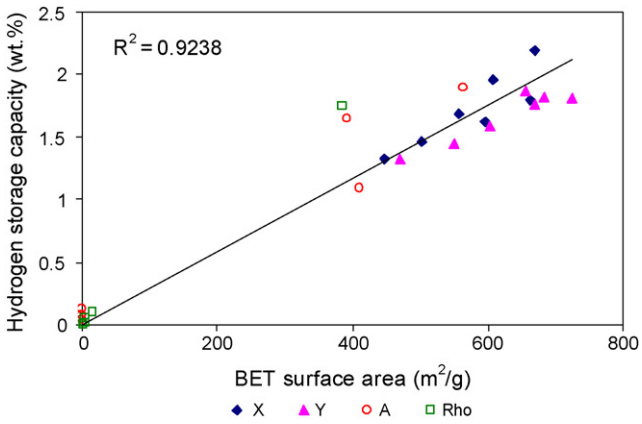

Fig. 9. Correlation between hydrogen storage capacity and BET surface area for zeolites X, Y, A and Rho. The correlation coefficient is also indicated. Reprinted with permission from [111]. Copyright 2005 Elsevier.

Recently, Vitillo et al. [112] carried out a theoretical investigation to estimate the maximum amount of molecular hydrogen that could be placed in the pores of various zeotypes. Among the systems investigated, the highest maximal capacities obtained was 2.86 mass% for systems with the FAU and RHO frameworks. Though zeolites are an interesting and highly varied class of inorganic materials, their hydrogen storage capacities are low, and they generally fall short of the 6 wt.% target described in the introduction.

6. Summary

We have reviewed the potential of four inorganic materials or systems; namely lithium nitride, ammonia borane, carbon nanotubes and zeolites, as hydrogen storage media in a hydrogen economy. None of these currently satisfies all of the US DOE requirements for a practical hydrogen storage system for transportation. Though lithium nitride has high gravimetric hydrogen storage capacity with good reversibility, the temperature for hydrogen absorption/desorption is high. Ammonia borane has a very high hydrogen content and low desorption temperature, but suffers from irreversibility and from the release of other gaseous products along with H_2 during decomposition. Carbon nanotubes have been reported to show potentially acceptable wt.% values for hydrogen uptake, but there is major disagreement in the literature regarding some of the higher values and their reproducibility. Furthermore, the lack of a rational chemical synthesis of these materials poses a major obstacle to their development as hydrogen storage materials. Zeolites are advantageous in that they are cheap, easy to synthesize, stable, and non-flammable in air or hydrogen, but their main drawback is that the gravimetric hydrogen storage capacity is low and any significant hydrogen uptake occurs at very low temperatures

or high pressures. Notwithstanding the issues which currently bedevil their use, lithium nitride and carbon nanotubes appear to have the most potential for a breakthrough which may lead to viability in terms of hydrogen storage: discovery of a suitable dopant, which can change the thermodynamics of lithium nitride sufficiently to lower the absorption and desorption temperatures by 50–100 °C would bring this system within reach of the US DOE criteria; and the development of a higher yield synthesis – ideally a rational chemical route – would open the way for carbon nanotubes to fulfil much of the promise that surrounded their discovery in the 1990s.

References

[1] US Department of Energy, Office of Basic Energy Sciences, Basic Research Needs for the Hydrogen Economy, US DOE, Washington, DC, 2004. Available at http://www.sc.doe.gov/bes/hydrogen.pdf.
[2] W. Grochala, P.P. Edwards, Chem. Rev. 104 (2004) 1283.
[3] S.R. Johnson, P.A. Anderson, P.P. Edwards, I. Gameson, J.W. Prendergast, M. Al-Mamouri, D. Book, I.R. Harris, S.J. Speight, A. Walton, Chem. Commun. 22 (2005) 2823.
[4] J.M. Bellosta von Colbe, M. Felderhoff, B. Bogdanovic, F. Schuth, C. Weidenthaler, Chem. Commun. 37 (2005) 4732.
[5] F. Schüth, B. Bogdanovi, M. Felderhoff, Chem. Commun. 20 (2004) 2249.
[6] F.W. Dafert, R. Miklauz, Monatsch. Chem. 31 (1910) 981.
[7] P. Chen, Z. Xiong, J. Luo, J. Lin, K.L. Tan, Nature 420 (2002) 302.
[8] Y.H. Hu, N.Y. Yu, E. Ruckenstein, Ind. Eng. Chem. Res. 43 (2004) 4174.
[9] D.H. Gregory, Coord. Chem. Rev. 215 (2001) 301.
[10] E. Zintl, G. Brauer, Z. Elektrochem, Angew. Phys. Chem. 41 (1935) 102.
[11] A. Rabenau, H. Schulz, J. Less-Comm. Met. 50 (1976) 155.
[12] J.O. Thomas, R. Tellgren, Solid State Ionics 5 (1981) 407.
[13] Y.H. Hu, E. Ruckenstein, Ind. Eng. Chem. Res. 42 (2003) 5135.
[14] G.P. Meisner, F.E. Pinkerton, M.S. Meyer, M.P. Balogh, M.D. Kundrat, J. Alloys Compd. 404–406 (2005) 24.
[15] Y.H. Hu, N.Y. Yu, E. Ruckenstein, Ind. Eng. Chem. Res. 44 (2005) 4304.
[16] Y.H. Hu, E. Ruckenstein, J. Phys. Chem. A 107 (2003) 9737.
[17] Y.H. Hu, E. Ruckenstein, Ind. Eng. Chem. Res. 43 (2004) 2464.
[18] Y.H. Hu, E. Ruckenstein, Ind. Eng. Chem. Res. 44 (2005) 1510.
[19] P. Chen, Z. Xiong, J. Luo, J. Lin, K.L. Tan, J. Phys. Chem. B 107 (2003) 10967.
[20] S. Hino, T. Ichikawa, N. Ogita, M. Udagawa, H. Fujii, Chem. Commun. 24 (2005) 3038.
[21] T. Ichikawa, N. Hanada, S. Isobe, H.Y. Leng, H. Fujii, J. Alloys Compd. 404–406 (2005) 435.
[22] F.E. Pinkerton, J. Alloys Compd. 400 (2005) 76.
[23] T. Ichikawa, S. Isobe, N. Hanada, H. Fujii, J. Alloys Compd. 365 (2004) 271.
[24] S. Isobe, T. Ichikawa, N. Hanada, H.Y. Leng, M. Fichtner, O. Fuhr, H. Fujii, J. Alloys Compd. 404–406 (2005) 439.
[25] K. Miwa, N. Ohba, S. Towata, Phys. Rev. B 71 (2005) 195109.
[26] S. Orimo, Y. Nakamori, G. Kitahara, K. Miwa, N. Ohba, T. Noritake, S. Towata, Appl. Phys. A 79 (2004) 1765.
[27] W. Luo, J. Alloys Compd. 381 (2004) 284.
[28] Y. Nakamori, S. Orimo, Mater. Sci. Eng. B 108 (2004) 48.
[29] T. Ichikawa, K. Tokoyoda, H. Leng, H. Fujii, J. Alloys Compd. 400 (2005) 245.
[30] H.Y. Leng, T. Ichikawa, S. Isobe, S. Hino, N. Hanada, H. Fujii, J. Alloys Compd. 404–406 (2005) 443.
[31] H. Leng, T. Ichikawa, S. Hino, T. Nakagawa, H. Fujii, J. Phys. Chem. B 109 (2004) 10744.
[32] Y. Nakamori, G. Kitahara, S. Orimo, J. Power Sources 138 (2004) 309.
[33] W. Luo, S. Sickafoose, J. Alloys Compd. 407 (2006) 274.
[34] Z. Xiong, J. Hu, G. Wu, P. Chen, J. Alloys Compd. 395 (2005) 209.
[35] S. Hino, T. Ichikawa, H. Leng, H. Fujii, J. Alloys Compd. 398 (2005) 62.
[36] M. Aoki, K. Miwa, T. Noritake, G. Kitahara, Y. Nakamori, S. Orimo, S Towata, Appl. Phys. A 80 (2005) 1409.
[37] F.E. Pinkerton, G.P. Meisner, M.S. Meyer, M.P. Balogh, M.D. Kundrat, J. Phys. Chem. B 109 (2005) 6.
[38] J. Lu, Z.Z. Fang, J. Phys. Chem. B 109 (2005) 20830.
[39] A. Gutowska, L. Li, Y. Shin, C.M. Wang, X.S. Li, J.C. Linehan, R.S. Smith, B.D. Kay, B. Schmid, W. Shaw, M. Gutowska, T. Autrey, Angew. Chem. Int. Ed. 44 (2005) 3578.
[40] K.W. Böddeker, S.G. Shore, R.K. Bunting, J. Am. Chem. Soc. 88 (1966) 4396.
[41] W.T. Klooster, T.F. Koetzle, P.E.M. Siegbahn, T.B. Richardson, R.H. Crabtree, J. Am. Chem. Soc. 121 (1999) 6337.
[42] R.W. Parry, D.R. Schultz, P.R. Girardot, J. Am. Chem. Soc. 80 (1958) 1.
[43] S.G. Shore, R.W. Parry, J. Am. Chem. Soc. 77 (1955) 6084.
[44] S.G. Shore, R.W. Parry, J. Am. Chem. Soc. 80 (1958) 8.
[45] R.H. Crabtree, P.E.M. Siegbahn, O. Eisenstein, A.L. Rheingold, T.F. Koetzle, Acc. Chem. Res. 29 (1996) 348.
[46] M.G. Hu, R.A. Geanangel, W.W. Wendlandt, Thermochim. Acta 23 (1978) 249.
[47] G. Wolf, J. Baumann, F. Baitalow, F.P. Hoffmann, Thermochim. Acta 243 (2000) 19.
[48] F. Baitalow, J. Baumann, G. Wolf, K. Jaenicke-Röβler, G. Leitner, Thermochim. Acta 391 (2002) 159.
[49] J. Baumann, F. Baitalow, G. Wolf, Thermochim. Acta 430 (2005) 9.
[50] V. Sit, R.A. Geanangel, W.W. Wendlandt, Thermochim. Acta 113 (1987) 379.
[51] M.G. Hu, J.M. van Paasschen, R.A. Geanangel, J. Inorg. Nucl. Chem. 39 (1977) 2147.
[52] C.T. Kwon, H.A. McGee Jr., Inorg. Chem. 9 (1970) 2438.
[53] E.R. Lory, R.F. Porter, J. Am. Chem. Soc. 95 (1973) 1766.
[54] J. Huober, M. Pfeffer, A. Ruoff, Z. Anorg, Allg. Chem. 627 (2001) 589.
[55] R. Komm, R.A. Geanangel, R. Liepins, Inorg. Chem. 22 (1983) 1684.
[56] S.D. Benedetto, M. Carewska, C. Cento, P. Gibson, M. Pasquali, S. Scaccia, P.P. Prosini, Thermochim. Acta 441 (2006) 184.
[57] M.S. Dresselhaus, Annu. Rev. Mater. Sci. 27 (1997) 1.
[58] A. Thess, R. Lee, P. Nikolaev, H. Dai, P. Petit, J. Robert, C. Xu, Y.H. Lee, S.G. Kim, A.G. Rinzler, D.T. Colbert, G.E. Scuseria, D. Tomanek, J.E. Fisher, R.E. Smalley, Science 273 (1996) 483.
[59] S. Iijima, Nature 356 (1991) 56.
[60] S. Iijima, T. Ichihashi, Nature 363 (1993) 603.
[61] A. Züttel, P. Wenger, P. Sudan, P. Mauron, S. Orimo, Mater. Sci. Eng. B 108 (2004) 9.
[62] A.C. Dillon, M.J. Heben, Appl. Phys. A 72 (2001) 133.
[63] C. Liu, H. Cheng, J. Phys. D: Appl. Phys. 38 (2005) R231.
[64] M. Rzepka, P. Lamp, M.A. de la Casa-Lillo, J. Phys. Chem. B 102 (1998) 10894.
[65] Q. Wang, J.K. Johnson, J. Chem. Phys. 110 (1999) 577.
[66] K.F. Darkrim, D. Levesque, J. Phys. Chem. B 104 (2000) 6773.
[67] S.M. Lee, Y.H. Lee, Appl. Phys. Lett. 76 (2000) 2877.
[68] R.F. Cracknell, Mol. Phys. 100 (2002) 2079.
[69] Y. Ma, Y. Xia, M. Zhao, M. Ying, Phys. Rev. B 65 (2002) 155430.
[70] P. Guay, B.L. Stansfield, A. Rochefort, Carbon 42 (2004) 2187.
[71] S.M. Lee, K.S. Park, Y.C. Choi, Y.S. Park, J.M. Bok, D.J. Bae, K.S. Nahm, Y.G. Choi, S.C. Yu, N. Kim, T. Frauenheim, Y.H. Lee, Synth. Met. 113 (2000) 209.
[72] V.V. Simonyan, J.K. Johnson, J. Alloys Compd. 330–332 (2002) 659.
[73] A. Züttel, Ch. Nützenadel, P. Sudan, Ph. Mauron, Ch. Emmenegger, S. Rentsch, L. Schlapbach, A. Weidenkaff, T. Kiyobayashi, J. Alloys Compd. 330–332 (2002) 676.
[74] A. Züttel, P. Sudan, Ph. Mauron, T. Kiyobayashi, Ch. Emmenegger, L. Schlapbach, Int. J. Hydrogen Energy 27 (2002) 203.
[75] A.C. Dillon, K.M. Jones, T.A. Bekkedahl, C.H. Klang, D.S. Bethune, M.J. Heben, Nature 386 (1997) 377.
[76] Y. Ye, C.C. Ahn, C. Witham, B. Fultz, J. Liu, A.G. Rinzler, D. Colbert, K.A. Smith, R.E. Smalley, Appl. Phys. Lett. 74 (1999) 2307.
[77] A.C. Dillon, T. Gennett, J.L. Alleman, K.M. Jones, P.A. Parilla, M.J. Heben, DOE/NREL Hydrogen Program Review, May 8–10, 2000.

[78] M. Hirscher, M. Becher, M. Haluska, U. Detlaff-Weglikowska, A. Quintel, G.S. Duesberg, Y.-M. Choi, P. Downes, M. Hulman, S. Roth, I. Stepanek, P. Bernier, Appl. Phys. A 72 (2001) 129.
[79] C. Liu, Y.Y. Fan, M. Liu, H.I. Cong, H.M. Cheng, M.S. Dresselhaus, Science 286 (1999) 1127.
[80] A. Chambers, C. Park, R.T.K. Baker, N.M. Rodriguez, J. Phys. Chem. B 102 (1998) 4253.
[81] C.C. Ahn, Y. Ye, B.V. Ratnakumar, C. Witham, R.C. Bowman Jr., B. Fultz, Appl. Phys. Lett. 73 (1998) 3378.
[82] R. Ströbel, L. Jörissen, T. Schliermann, V. Trapp, W. Schutz, K. Bohmhammel, G. Wolf, J. Garche, J. Power Sources 84 (1999) 221.
[83] P. Chen, X. Wu, J. Lin, K.L. Tan, Science 285 (1999) 91.
[84] R.T. Yang, Carbon 38 (2000) 623.
[85] M. Hirscher, M. Becher, M. Haluska, A. Quintel, V. Skakalova, Y. Choi, U. Detlaff-Weglikowska, S. Roth, I. Stepanek, P. Bernier, A. Leonhardt, J. Fink, J. Alloys Compd. 330–332 (2002) 654.
[86] X.B. Wu, P. Chen, J. Lin, K.L. Tan, Int. J. Hydrogen Energy 25 (2000) 261.
[87] E. Poirier, R. Chahine, P. Benard, D. Cossement, L. Lafi, E. Melancon, T.K. Bose, S. Desilets, Appl. Phys. A 79 (2004) 961.
[88] A. Lan, A. Mukasyan, J. Phys. Chem. B 109 (2005) 16011.
[89] B. Panella, M. Hirscher, S. Roth, Carbon 43 (2005) 2209.
[90] S. Yamanaka, M. Fujikane, M. Uno, H. Murakami, O. Miura, J. Alloys Compd. 366 (2004) 264.
[91] R.M. Barrer, Zeolites and Clay Minerals as Sorbents and Molecular Sieves, Academic Press, London, 1978.
[92] H.W. Langmi, A. Walton, M.M. Al-Mamouri, S.R. Johnson, D. Book, J.D. Speight, P.P. Edwards, I. Gameson, P.A. Anderson, I.R. Harris, J. Alloys Compd. 356–357 (2003) 710.
[93] A. Dyer, An Introduction to Zeolite Molecular Sieves, Wiley, Chichester, 1988.
[94] D. Fraenkel, J. Shabtai, J. Am. Chem. Soc. 99 (1977) 7074.
[95] J. Weitkamp, M. Fritz, S. Ernst, Int. J. Hydrogen Energy 30 (1995) 967.
[96] D. Fraenkel, J. Am. Chem. Soc. Faraday Trans. 1 77 (1981) 2029.
[97] D. Fraenkel, J. Am. Chem. Soc. Faraday Trans. 1 77 (1981) 2041.
[98] J. Yoon, N.H. Heo, J. Phys. Chem. 96 (1992) 4997.
[99] J. Yoon, J. Phys. Chem. 97 (1993) 6066.
[100] V.V. Krishnan, S.L. Suib, D.R. Corbin, S. Schwarz, G.E. Jones, Catal. Today 31 (1996) 199.
[101] F. Darkrim, A. Aoufi, P. Malbrunot, J. Chem. Phys. 112 (2000) 5991.
[102] N. Nishimiya, T. Kishi, T. Mizushima, A. Matsumoto, K. Tsutsumi, J. Alloys Compd. 319 (2001) 312.
[103] S.B. Kayiran, F.L. Darkrim, Surf. Interf. Anal. 34 (2002) 100.
[104] V.B. Kazansky, V.Y. Borovkov, H.G. Karge, Micropor. Mesopor. Mat. 22 (1998) 251.
[105] V.B. Kazansky, F.C. Jentoft, H.G. Karge, J. Am. Chem. Soc. Faraday Trans. 94 (1998) 1347.
[106] V.B. Kazansky, J. Mol. Catal. A: Chem. 141 (1999) 83.
[107] X. Solans-Monfort, V. Branchadell, M. Sodupe, C.M. Zicovich-Wilson, E. Gribov, G. Spoto, C. Busco, P. Ugliengo, J. Phys. Chem. B 108 (2004) 8278.
[108] A. Zecchina, S. Bordiga, J.G. Vitillo, G. Ricchiardi, C. Lambert, G. Spoto, M. Bjørgen, K.P. Lillerud, J. Am. Chem. Soc. 127 (2005) 6361.
[109] L. Regli, A. Zecchina, J.G. Vitillo, D. Cocina, G. Spoto, C. Lamberti, K.P. Lillerud, U. Olsbye, S. Bordiga, Phys. Chem. Chem. Phys. 7 (2005) 3197.
[110] M.G. Nijkamp, J.E.M.J. Raaymakers, A.J. van Dillen, K.P. de Jong, Appl. Phys. A 72 (2001) 619.
[111] H.W. Langmi, D. Book, A. Walton, S.R. Johnson, M.M. Al-Mamouri, J.D. Speight, P.P. Edwards, I.R. Harris, P.A. Anderson, J. Alloys Compd. 404–406 (2005) 637.
[112] J.G. Vitillo, G. Ricchiardi, G. Spoto, A. Zecchina, Phys. Chem. Chem. Phys. 7 (2005) 3948.